Supplement of Atmos. Meas. Tech., 14, 355–367, 2021
https://doi.org/10.5194/amt-14-355-2021-supplement

Atmospheric Measurement Techniques
Open Access
EGU

Supplement of

On the calibration of FIGAERO-ToF-CIMS: importance and impact of calibrant delivery for the particle-phase calibration

Arttu Ylisirniö et al.

Correspondence to: Arttu Ylisirniö (arttu.ylisirnio@uef.fi) and Siegfried Schobesberger (siegfried.schobesberger@uef.fi)

S1. Different P_{sat} values used in FIGAERO-ToF-CIMS calibrations in different studies

Table S1. Collection of literature-based P_{sat} (Pa) values used in various published FIGAERO calibrations, P_{sat} values used in this study are taken from Lopez-Hilfiker et al., (2014).

Saturation pressure (Pa)	**Lopez-Hilfiker et al., (2014)**	**Stark et al., (2017)**	**Nah et al., (2019)**	**Bannan et al., (2019)**	**Ye et al., (2019)**	**(Wang et al., 2020)**	**This study**
Glutaric acid		6.7×10^{-4}	1×10^{-3}	1×10^{-3}	4×10^{-4}	2.6×10^{-4}	
Cis-Pinonic acid	6×10^{-5}	0.03	7.8×10^{-4}	7.79×10^{-4}			
Pimelic acid	1.3×10^{-4}		2.6×10^{-4}				1.3×10^{-4}
Erythritol			6.3×10^{-5}				
Palmitic acid	1.4×10^{-4}		2.0×10^{-5}		5×10^{-5}	2.8×10^{-5}	1.4×10^{-4}
Azelaic acid	6×10^{-6}	6×10^{-6}	7.4×10^{-6}			1.4×10^{-6}	6×10^{-6}
Oleic acid	1×10^{-6}						
Stearic acid	1×10^{-5}		2.5×10^{-6}				1×10^{-6}
Sebacic acid	1.5×10^{-6}		1.5×10^{-6}				1.5×10^{-6}
Behenic acid	7×10^{-4}		4.9×10^{-8}				
Oleic acid	1×10^{-5}						1×10^{-5}
Tricarballylic acid		3×10^{-7}			3.1×10^{-7}	3.1×10^{-7}	
Pinic acid	6×10^{-5}	4.3×10^{-5}		3.2×10^{-5}	9.3×10^{-5}		
Citric acid					2.7×10^{-10}	2.7×10^{-10}	
Camphoric acid					2×10^{-4}	2×10^{-5}	
Dodecanoic/lauric acid					0.01		
Succinic acid				1.3×10^{-3}			
Malonic acid				6.2×10^{-4}			
Adipic acid				1.8×10^{-4}			
Suberic acid				2.23×10^{-5}			

S2. Measurement schematics

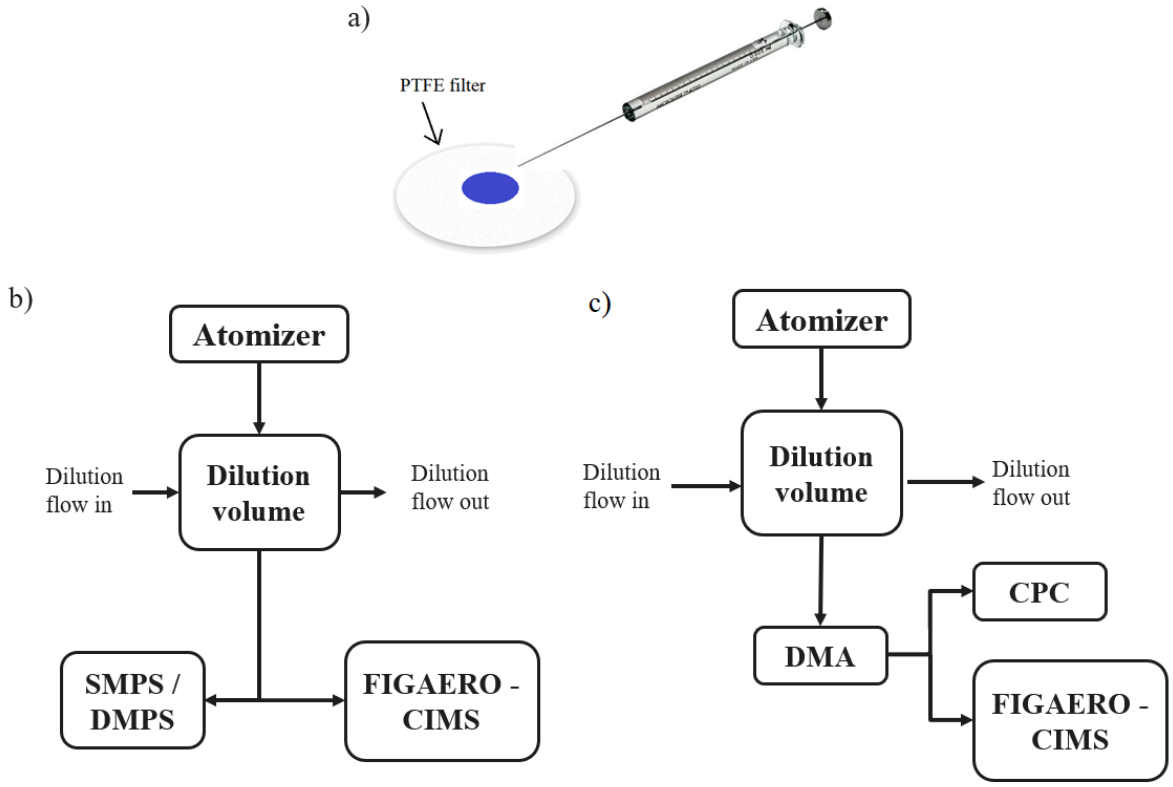

Figure S1. Panel a) illustration of the syringe deposition method. Measurement setup schematics for the atomizer method either with b) polydisperse particles or c) monodisperse particles. The dilution volume is used in the atomizer method to ensure complete evaporation of the solvent before particle characterization.

S3. Measured T_{max} values

Table S2. Average T_{max} values (˚C) and standard deviations based on three repetitions, as shown in Figure 3 panel a). Used P_{sat} (Pa), based on Krieger et al., (2018)*, are shown in the bottom row.*

Experiment	**PEG-4**	**PEG-5**	**PEG-6**	**PEG-7**	**PEG-8**
Conc. 0.1 g L^{-1}	49.9±4.4	74.6 ± 3.1	94.6 ± 2.8	110.9 ± 2.4	123 ± 2
Conc. 0.01 g L^{-1}		38.5 ± 1.2	58.5 ± 1.5	76.8 ± 1.2	90.9 ± 0.9
Conc. 0.003 g L^{-1}		36.7 ± 1.9	57 ± 2.5	73.1 ± 2.9	88.7 ± 2.8
Atomizer		23.3 ± 0.5	39.9 ± 0.4	54.7 ± 0.4	65.5 ± 0.2
Saturation pressure (Pa)	0.0169	5.29×10^{-4}	3.05×10^{-5}	1.29×10^{-6}	9.2×10^{-8}

Table S3. Average T_{max} values (˚C) and standard deviations based on three repetitions, as shown in Figure 3 panel b). Used saturation pressure (Pa) values are shown in the bottom row.

Experiment	**Palmitic acid**	**Pimelic acid**	**Oleic acid**	**Azelaic acid**	**Stearic acid**	**Sebacic acid**
Conc. 0.5 g L^{-1}	55.8 ± 0.3	54 ± 0.1	61.8 ± 2.8	63.3 ± 0.3	64.7 ± 0.5	73.1 ± 0.1
Conc. 0.1 g L^{-1}	48.9 ± 1	46.1 ± 1.1	51.2 ± 1.8	54.8 ± 1.2	55.8 ± 1	62.6 ± 1.2
Conc. 0.01 g L^{-1}	40.6 ± 1.2	39.5 ± 2	43.9 ± 2.8	41.5 ± 1.5	44.8 ± 2.5	46.1 ± 0.4
Atomizer	36.6 ± 0.6	34 ± 0.4	34.7 ± 0.8	40.2 ± 0.7	43.5 ± 0.6	49.4 ± 1
Saturation pressure (Pa)	1.4 x 10^{-4}	1.3 x 10^{-4}	1 x 10^{-5}	6 x 10^{-6}	1 x 10^{-6}	1.47 x 10^{-6}

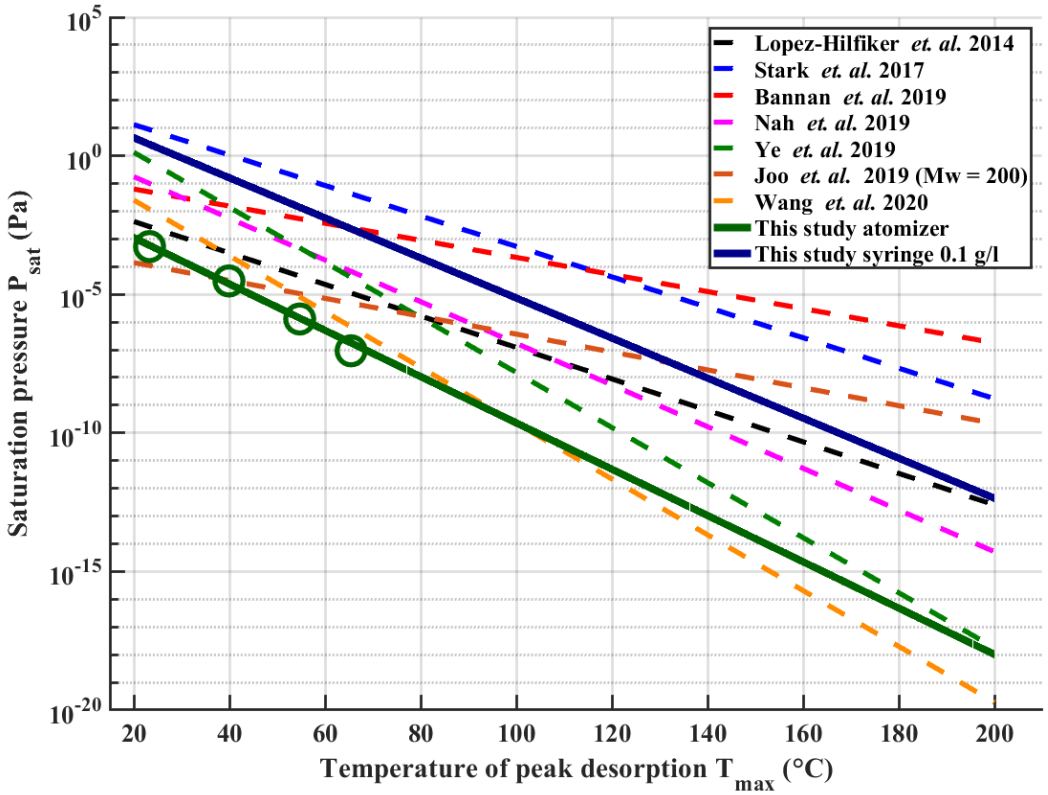

Figure S2. Repeated Fig. 1 (dashed lines) with calibration lines from this study added for the atomizer method (green solid line) and the syringe method (for a solution concentration of 0.1 g L^{-1}, solid blue line). Both lines are for 30 min ramping times and the atomizer measurements used polydisperse aerosol with a median particle size of 60 nm. Green circles show the measured data where the line have been fitted.

S4. Error analysis for Figure 8.

Errors for deposited mass on the filter shown in Fig.8 are determined with propagation of error for both methods. For syringe deposition the equation is of the form

$$m_{syringe} = V_s C_s,$$

where V_s (ml) is the injected volume and C_s (g l^{-1}) is the mass concentration of the solution. The solution was prepared by weighting the analyte with a microscale and solving it to 200 ml of ACN to make 0.2 g/l solution. The stock solution was then diluted into 50ml solution of 0.01 g/l concentration. To account for the dilution, the equation now becomes to form

$$m_{syringe} = \frac{V_{syr}V_{pip}}{V_{fin}V_{sto}} m_{scale},$$

where V_{syr} is deposited volume to the filter, V_{pip} is volume pipetted from stock solution to make the dilute solution, V_{fin} is the volume final dilute solution, V_{sto} is the volume of the stock solution and m_{scale} is the analytes mass measured with the microscale. Now denoting

$$R = \frac{V_{syr}V_{pip}}{V_{fin}V_{sto}}$$

we get the equation to the form

$$m_{syr} = R\, m_{scale}$$

and formula for propagation of error becomes

$$\Delta \mathrm{m}_{\mathrm{syringe}} = \sqrt{\left(\frac{\partial m_{syr}}{\partial R}\right)^2 \Delta R^2 + \left(\frac{\partial m_{syr}}{\partial m_{scale}}\right)^2 \Delta {m_{scale}}^2},$$

$$\Delta \mathrm{m}_{\mathrm{syringe}} = \sqrt{{\mathrm{m}_{\mathrm{scale}}}^2 \Delta R^2 + R^2 \Delta {m_{scale}}^2},$$

where

$$\Delta R = \sqrt{\left(\frac{V_{pip}}{V_{fin}V_{sto}}\right)^2 \Delta {V_{syr}}^2 + \left(\frac{V_{syr}}{V_{fin}V_{sto}}\right)^2 \Delta {V_{pip}}^2 + \left(-\frac{V_{syr}V_{pip}}{V_{fin}^2 V_{sto}}\right)^2 \Delta {V_{fin}}^2 + \left(-\frac{V_{syr}V_{pip}}{V_{fin}V_{sto}^2}\right)^2 \Delta {V_{sto}}^2}.$$

When using Class A glassware, tolerances for different measurement flasks can be found online.

Atomizer deposition

Amount of deposited particulate mass can be calculated with equation

$$m_{atom} = FtV_c,$$

where F is the flow through the filter [m^3 s^{-1}], t [s] is the collection time and V_c [µg m^{-3}] is the particle mass concentration in the sample air. The propagation of error formula for this equation is of the form

$$\Delta \mathrm{m}_{\mathrm{atom}} = \sqrt{\left(\frac{\partial m_{atom}}{\partial F}\right)^2 \Delta F^2 + \left(\frac{\partial m_{atom}}{\partial t}\right)^2 \Delta t^2 + \left(\frac{\partial m_{atom}}{\partial V_c}\right)^2 \Delta {V_c}^2},$$

$$\Delta \mathrm{m}_{\mathrm{atom}} = \sqrt{(tV_c)^2 \Delta F^2 + (FV_c)^2 \Delta t^2 + (Ft)^2 \Delta {V_c}^2},$$

where ΔF = 0.01 x F (flow meter accuracy), Δt = 1 (assuming swift movement of the tray). When using monodisperse aerosol sampling method as shown in Fig. S1 b), particle mass concentration can be calculated by assuming spherical particle shape as

$$V_c = \frac{\rho d_p^3 \pi n}{6},$$

where ρ is the density of the aerosol particles, d_p is the set monodisperse particle size and n is particle number concentration measured with CPC. The uncertainty of V_c is then

$$\Delta V_c = \sqrt{\left(\frac{3\rho d_p^2 \pi}{6}\right)^2 \Delta d_p^2 + \left(\frac{\rho d_p^3 \pi}{6}\right)^2 \Delta n^2},$$

where Δd_p = 0.01 x d_p and Δn = 0.1 x n with instrumentation described in Sect. 2.4.

Y-axis errors for Figure 8 are calculated by assuming Poisson-type measurement error for CIMS measurements (Yan et al., 2016)

$$e_i = \sqrt{\frac{S_i}{\Delta t}} + a,$$

where S_i is the measured signal, Δt is the difference of two-time steps and a is constant accounting for electrical noise.

When integrating over such data, we assumed error to be of the form

$$\Delta I = \pm 1.96 \sqrt{std(S)^2 + \sum e_i^2},$$

where *std(S)* is the standard deviation over the whole thermogram.

S5. P_{sat} of higher order PEGs

We performed additional T_{max} measurements of an atomized PEG-400 solution (Sigma Aldrich), which contains different PEGs so that the average molecular mass of the solution is about 400 g/mol. Detected PEGs ranged from PEG-6 to PEG-16. Fig. S3 a) shows measured T_{max} values of different PEGs versus the molecular mass of the compounds. The measured points follow well a second order polynomial fitted to the points. It should be noted that T_{max} values of PEG-400 are about 5-7 ˚C higher than values measured for individual PEGs, possibly due to additional stabilization compounds in the product. Figure S3 b) shows a somewhat bold log-linear extrapolation of saturation pressures from measured PEGs (4-8) up to PEG-16.

In Fig S3 c) we show two extrapolations for P_{sat} vs. measured T_{max}. Extrapolation a) was done by substituting T_{max} values in eq. (2) with the polynomial fit to molecular mass ($T_{max} = d\ Mw^2 + e\ Mw + f$, where Mw is molecular weight and d, e and f are fitted constants), shown in Fig. S3a, while using fit coefficients a and b from eq. (2). I.e., extrapolation a) estimates P_{sat} values based on molecular mass.

Extrapolation b) was done by directly fitting the normal logarithm of P_{sat} vs molecular mass (Fig. S3 b).

As can be seen, the two extrapolation methods for P_{sat} lead to substantially different extended calibration curves in the higher desorption temperatures. Our results anyhow strongly suggest that higher order PEGs could be used for extending the volatility calibration range, if their saturation vapor pressures were established by accurate independent measurements or estimated with high enough certainty.

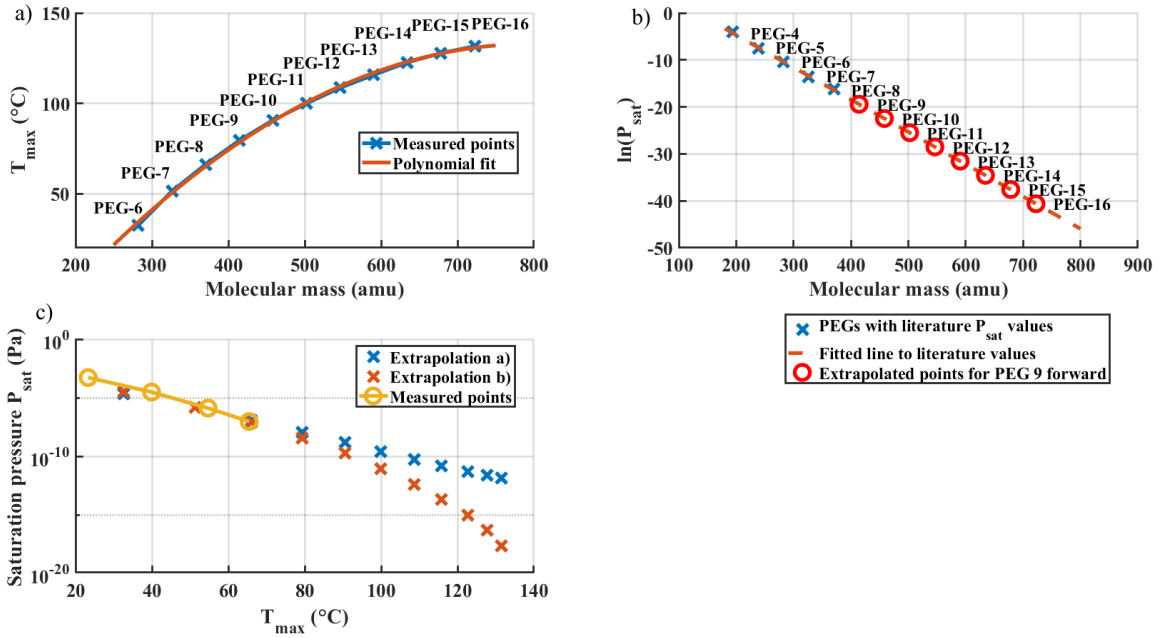

Figure S3. Panel a) measured T_{max} values (crosses) vs. molecular mass of the PEGs contained in the PEG-400 mixture, and a polynomial fit applied to the data. Panel b) natural logarithm of saturation pressure vs. PEG molecular mass, and a linear fit to the literature-supported data sub-set (crosses), extrapolated to extend to all other PEGs (circles). Panel c) saturation pressure P_{sat} vs T_{max} extrapolated to cover all PEG, using extrapolations based on the fitted functions in panels a) and b).

References

Bannan, T. J., Le Breton, M., Priestley, M., Worrall, S. D., Bacak, A., Marsden, N. A., Mehra, A., Hammes, J., Hallquist, M., Alfarra, M. R., Krieger, U. K., Reid, J. P., Jayne, J., Robinson, W., McFiggans, G., Coe, H., Percival, C. J. and Topping, D.: A method for extracting calibrated volatility information from the FIGAERO-HR-ToF-CIMS and its experimental application, Atmos. Meas. Tech., 12(3), 1429–1439, doi:10.5194/amt-12-1429-2019, 2019.

Krieger, U. K., Siegrist, F., Marcolli, C., Emanuelsson, E. U., Gøbel, F. M., Bilde, M., Marsh, A., Reid, J. P., Huisman, A. J., Riipinen, I., Hyttinen, N., Myllys, N., Kurtén, T., Bannan, T., Percival, C. J. and Topping, D.: A reference data set for validating vapor pressure measurement techniques: Homologous series of polyethylene glycols, Atmos. Meas. Tech., 11(1), 49–63, doi:10.5194/amt-11-49-2018, 2018.

Lopez-Hilfiker, F. D., Mohr, C., Ehn, M., Rubach, F., Kleist, E., Wildt, J., Mentel, T. F., Lutz, A., Hallquist, M., Worsnop, D. and Thornton, J. A.: A novel method for online analysis of gas and particle composition: Description and evaluation of a filter inlet for gases and AEROsols (FIGAERO), Atmos. Meas. Tech., 7(4), 983–1001, doi:10.5194/amt-7-983-2014, 2014.

Nah, T., Xu, L., Osborne-Benthaus, K. A., White, S. M., France, S. and Lee Ng, N.: Mixing order of sulfate aerosols and isoprene epoxydiols affects secondary organic aerosol formation in chamber experiments, Atmos. Environ., 217(August), doi:10.1016/j.atmosenv.2019.116953, 2019.

Stark, H., Yatavelli, R. L. N., Thompson, S. L., Kang, H., Krechmer, J. E., Kimmel, J. R., Palm, B. B., Hu, W., Hayes, P. L., Day, D. A., Campuzano-Jost, P., Canagaratna, M. R., Jayne, J. T., Worsnop, D. R. and Jimenez, J. L.: Impact of Thermal Decomposition on Thermal Desorption Instruments: Advantage of Thermogram Analysis for Quantifying Volatility Distributions of Organic Species, Environ. Sci. Technol., 51(15), 8491–8500, doi:10.1021/acs.est.7b00160, 2017.

Wang, M., Chen, D., Xiao, M., Ye, Q., Stolzenburg, D., Hofbauer, V., Ye, P., Vogel, A. L., Mauldin, R. L., Amorim, A., Baccarini, A., Baumgartner, B., Brilke, S., Dada, L., Dias, A., Duplissy, J., Finkenzeller, H., Garmash, O., He, X. C., Hoyle, C. R., Kim, C., Kvashnin, A., Lehtipalo, K., Fischer, L., Molteni, U., Petäjä, T., Pospisilova, V., Quéléver, L. L. J., Rissanen, M., Simon, M., Tauber, C., Tomé, A., Wagner, A. C., Weitz, L., Volkamer, R., Winkler, P. M., Kirkby, J., Worsnop, D. R., Kulmala, M., Baltensperger, U., Dommen, J., El-Haddad, I. and Donahue, N. M.: Photo-oxidation of Aromatic Hydrocarbons Produces Low-Volatility Organic Compounds, Environ. Sci. Technol., 54(13), 7911–7921, doi:10.1021/acs.est.0c02100, 2020.

Yan, C., Nie, W., Aïjälä, M., Rissanen, M. P., Canagaratna, M. R., Massoli, P., Junninen, H., Jokinen, T., Sarnela, N., Häme, S. A. K., Schobesberger, S., Canonaco, F., Yao, L., Prévôt, A. S. H., Petäjä, T., Kulmala, M., Sipilä, M., Worsnop, D. R. and Ehn, M.: Source characterization of highly oxidized multifunctional compounds in a boreal forest environment using positive matrix factorization, Atmos. Chem. Phys., 16(19), 12715–12731, doi:10.5194/acp-16-12715-2016, 2016.

Ye, Q., Wang, M., Hofbauer, V., Stolzenburg, D., Chen, D., Schervish, M., Vogel, A., Mauldin, R. L., Baalbaki, R., Brilke, S., Dada, L., Dias, A., Duplissy, J., El Haddad, I., Finkenzeller, H., Fischer, L., He, X., Kim, C., Kürten, A., Lamkaddam, H., Lee, C. P., Lehtipalo, K., Leiminger, M., Manninen, H. E., Marten, R., Mentler, B., Partoll, E., Petäjä, T., Rissanen, M., Schobesberger, S., Schuchmann, S., Simon, M., Tham, Y. J., Vazquez-Pufleau, M., Wagner, A. C., Wang, Y., Wu, Y., Xiao, M., Baltensperger, U., Curtius, J., Flagan, R., Kirkby, J., Kulmala, M., Volkamer, R., Winkler, P. M., Worsnop, D. and Donahue, N. M.: Molecular Composition and Volatility of Nucleated Particles from α-Pinene Oxidation between -50 °c and +25 °c, Environ. Sci. Technol., 53(21), 12357–12365, doi:10.1021/acs.est.9b03265, 2019.